HHS Public Access

Author manuscript

Nat Chem. Author manuscript; available in PMC 2011 January 01.

Published in final edited form as:

Nat Chem. 2010 July ; 2(7): 558–565. doi:10.1038/nchem.660.

Triggering N_2 Uptake via Redox Induced Expulsion of Coordinated NH_3 and N_2 Silylation at Trigonal Bipyramidal Iron

Yunho Lee, **Neal P. Mankad**, and **Jonas C. Peters**

Department of Chemistry, Massachusetts Institute of Technology, Cambridge MA 02139

Abstract

The biological reduction of nitrogen to ammonia may occur via one of two predominant pathways in which nitrogenous N_xH_y intermediates including hydrazine (N_2H_4), diazene (N_2H_2), nitride (N^{3-}) and imide (NH^{2-}) may be involved. To test the validity of hypotheses concerning iron's direct role in the stepwise reduction of N_2, iron model systems are needed. Such systems can test the chemical compatibility of iron with various proposed N_xH_y intermediates, and the reactivity patterns of such species. Here we describe a TBP (SiP^R_3)Fe-L scaffold (SiP^R_3 represents [Si(*o*-$C_6H_4PR_2)_3]^-$; R = Ph and *i*Pr) where the apical site is occupied by nitrogenous ligands such as N_2, N_2H_4, NH_3 and N_2R. The system accommodates terminally bound N_2 in the three formal oxidation states (iron(0), +1, *and* +2). N_2 uptake is demonstrated via displacement of its reduction partners NH_3 and N_2H_4, and N_2 functionalizaton is illustrated via electrophilic silylation.

Recent work from our group and several others has targeted the synthesis of a variety of Fe-N_xH_y small molecule model complexes motivated by two goals.i,ii,iii,iv First and foremost is the desire to develop synthetic catalysts whose mode/s of action might relate to, or at least stimulate hypotheses concerning, the manner by which biological nitrogenases reduce N_2.v,vi,vii,viii Second, to be better positioned to interpret the spectroscopic data recently obtained for proposed intermediates of the N_2-ase cofactor there is a timely need to build a library of Fe-N_xH_y model complexes as a point of reference. Of specific interest to us are Fe-N_xH_y complexes whose iron centers reside in geometries that are either 4- or 5-coordinate and feature local three-fold symmetry where the N_xH_y can be viewed as occupying an axial site.ix,x Such geometries may be relevant to some if not all of the intermediates of iron-bound N_2 reduction cycles, as has been advanced elsewhere.v,xi

---

Correspondence to: Jonas C. Peters.

Author contributions

Y.L., N.P.M. and J.C.P. conceived and designed the experiments, Y.L. and N.P.M. performed the experiments and Y.L. and J.C.P. co-wrote the paper.

Additional information

Supplementary information and chemical sompound information accompany this paper at www.nature.com/naturechemistry. Reprints and permission information is available online at http://npg.nature.com/reprintsandpermissions/. Correspondence and requests for materials should be addressed to J.C.P.

With these goals in mind we have recently begun working with monoanionic tetradentate trisphosphinosilyl SiP^R_3 ligands (SiP^R_3 represents $[Si(o\text{-}C_6H_4PR_2)_3]^-$; R = Ph and *i*Pr) that accommodate mononuclear, *open-shell* 5-coordinate iron(II) and iron(I) species with a proclivity towards binding N_2 in the axial site of a trigonal bipyramid (TBP) at a position that is trans to the silyl anchor.xii,xvi Preliminary reactivity data established that protonation of N_2 can occur in modest yield to liberate N_2H_4.xii Hence, it became of interest to target hydrazine complexes and other open-shell iron complexes featuring nitrogenous ligands in the axial site. Established herein is that the (SiP^R_3)Fe template binds N_2 axially trans to the silyl anchor in three distinct oxidation states that can be represented formally as iron(0), +1, *and* +2. To our knowledge, no previously established transition metal system has been characterized that can accommodate terminal N_2 ligation across three oxidation states. In addition, the recycling of Fe(II)-NH_3 and Fe(II)-N_2H_4 complexes to Fe(I)-N_2 with expulsion of NH_3 is illustrated; this transformation is of interest as a key step of a hypothetical catalyst cycle where the iron(I) oxidation state is used to trigger N_2 uptake and NH_3 release. Finally, we also establish that it is possible to directly silylate the coordinated N_2 ligand to produce Fe-N_2SiR_3 products that appear to be far more stable than their Fe-N_2H counter-parts. This reactivity pattern, while well established for certain molybdenum systems, is not well known for iron.xiii In sum, these chemical properties add motivation to the search for a molecular N_2 reduction catalyst that uses iron as the redox active center to facilitate N_2 binding and reduction.

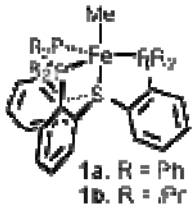

The most convenient means of entry to the chemistry described herein proceeds via the iron(II) methyl complexes (SiP^{Ph}_3)Fe(CH_3) (**1a**) and (SiP^{iPr}_3)Fe(CH_3) (**1b**). Addition of CH_3MgCl to a mixture of ferrous chloride with the corresponding silane H[SiP^R_3] in tetrahydrofuran at −78 °C, followed by stirring overnight at RT, affords the red *S* = 1 methyl complexes **1a** and **1b** in good yield. While these species can be isolated in relatively pure form, trace amounts of the (SiP^R_3)Fe(N_2) complex are typically present due to competitive reduction by CH_3MgCl. The solid-state structures of **1a** and **1b** have been determined (see SI for details) and show nearly ideal TBP geometries at the iron centers (τ = 0.91 for **1a** and 0.96 for **1b,** where τ = 0.00 for a perfect square pyramid and τ = 1.00 for a TBP geometryxiv). The solid-state structures are noteworthy in that the methyl ligands occupy axial sites trans to the silyl anchors (see SI). Cyclic voltammetry of **1a** reveals two reversible redox waves; $E_{1/2}$ = −0.57 and −2.3 V ($Fe^{III/II}$ and $Fe^{II/I}$ respectively; vs. Fc/Fc^+, see SI). Corresponding redox events for the isopropyl derivative **1b** are cathodically shifted by ~300 mV.

Synthesis and characterization of Fe-N_2, Fe-N_2^+, and Fe-N_2^-

Exposure of the methyl complexes to acid sources selectively releases methane. In THF solvent with $H(OEt_2)_2(B(ArF)_4)$ as the added acid ($B(ArF)_4$ = $B(3,5\text{-}(CF_3)_2\text{-}C_6H_3)_4$), **1a** is protonated to generate the cationic THF adduct $\{(SiP^{Ph}_3)Fe^{II}(THF)\}\{B(ArF)_4\}$, (**2a**). By contrast, exposure of the more electron releasing species **1b** to $H(OEt_2)_2(B(ArF)_4)$ under nitrogen favors formation of the cationic nitrogen complex $\{(SiP^{iPr}_3)Fe^{II}(N_2)\}\{B(ArF)_4\}$ (**3**) (Figure 1), which in THF solution under an atmosphere of nitrogen dominates the THF-adduct species by a ratio of ca. 6:1 as determined by UV-vis analysis. Alternatively, **3** can be obtained as a blue powder by adding $H(OEt_2)_2(B(ArF)_4)$ to a benzene solution of the red, previously reported N_2 adduct $(SiP^{iPr}_3)Fe(N_2)$ (**4b**).xvi GC analysis confirms H_2 as the byproduct of the latter reaction (see SI for details).

The presence of cationic $(SiP^{iPr}_3)Fe(N_2)^+$ species can also be gleaned by comparing the cyclic voltammetry of the neutral N_2 adduct $(SiP^{iPr}_3)Fe(N_2)$ (**4b**) under a nitrogen or argon atmosphere in THF solution. Figure 2 shows four traces. Trace (a) provides the cyclic voltammogram of **4b** under a nitrogen atmosphere. Two prominent and reversible waves are present at ca. -1.0 V and -2.2 V versus $FeCp_2/FeCp_2^+$. These are assigned as the Fe-N_2/Fe-N_2^+ and Fe-N_2/Fe-N_2^- waves, respectively. The wave at -1.0 V shows a small shoulder on its negative side (-1.1 V) that we presume arises due to the generation of Fe-THF^+ in addition to Fe-N_2^+ upon oxidation. As the sample is scanned cathodically a small feature appears at -1.9 V that we presume is due to the irreversible reduction of Fe-THF^+. Indeed, when **4b** is sparged for 30 sec with argon (b) the oxidation wave at -1.0 V corresponding to the oxidation of Fe-N_2 is no longer reversible because oxidation leads to rapid loss of N_2. Accordingly, the peak at -1.9 V increases in intensity because the generation of Fe-THF^+ is favored under argon. Re-admission of N_2 to the solution after removing most of the argon by rapid evacuation (c) gives rise to a partially recovered return wave at -1.0 V, which grows in intensity after thorough sparging with nitrogen (d) to provide a trace that is very similar to that observed initially (a), with the exception of a modest impurity appearing at ca. -1.7 V. One additional species to consider in the context of the assignments proposed above concerns trigonal pyramidal $(SiP^{iPr}_3)Fe$. The N_2 ligand of **4b** is modestly labile and it could therefore be that some of the minor features in the CV traces shown in Figure 2 arise from redox at such a 4-coordinate $(SiP^{iPr}_3)Fe$ species, for example the wave at -1.9 V. Our preference for assigning this latter wave to the reduction of Fe-THF^+ is in part due to the fact that when N_2 is removed (trace (b)) the solution color (orange) is that of other 5-coordinate and divalent $(SiP^{iPr}_3)Fe(L)^+$ species, for example the hydrazine adduct **6b** (vide infra).

We were gratified to find that the cationic complex **3** is sufficiently stable to be isolated and characterized. Its S = 1 spin state can be compared to that of its previously reported and nearly isostructural S = ½ relative **4b**.xii Sodium naphthelide reduction of **4b** affords the formally zerovalent congener $\{(SiP^{iPr}_3)Fe(N_2)\}\{Na(THF)_3\}$ (**5**). Addition of two equiv of 12-crown-4 to **5** encapsulates the Na^+ to provide terminally bonded $\{(SiP^{iPr}_3)Fe(N_2)\}\{Na(12\text{-}C\text{-}4)_2\}$ (**5'**). High resolution crystal structures have now been obtained for **3, 5**, and **5'** to accompany that which had been previously reported for **4b**. These structural data collectively afford the only such data available for a terminally bonded N_2 adduct of any

transition metal in three distinct oxidation states (Figure 3, Table 1). Schrock has reported that the trivalent molybednum dinitrogen adduct $[(HIPTNCH_2CH_2)_3N]Mo(N_2)$ (HIPT = 3,5-(2,4,6-*i*-$Pr_3C_6H_2)_2C_6H_3$) shows electrochemically reversible waves assigned as the Mo-$N_2^{+/0}$ and Mo-$N_2^{0/-}$, where the neutral and anionic derivatives have been structurally characterized, the latter as a Mg adduct.xv Key to note for the present iron system is that the N_2 ligand remains in the site trans to the Si anchor in each state of oxidation, and the iron center's geometry is preserved in the cationic, neutral, and anionic species. Structural changes worth noting include an Fe-N bond distance contraction as the system is successively reduced, and a corresponding Fe-Si contraction upon successive reduction (Table 1).

Synthesis and characterization of Fe-NH_3^+, Fe-$N_2H_4^+$, and Fe-$N_2H_3B(C_6F_5)_3$

The cationic THF and N_2 adducts are labile at the axial site trans to the silyl donor, and hence provide one pathway to the corresponding hydrazine adduct derivatives $\{(SiP^{Ph}_3)Fe^{II}(N_2H_4)\}\{B(ArF)_4\}$, {**6a**}{$B(ArF)_4$} and $\{(SiP^{iPr}_3)Fe^{II}(N_2H_4)\}\{B(ArF)_4\}$, {**6b**}{$B(ArF)_4$)} via N_2H_4 addition. Alternatively, slow addition of the hydrazinium acid $N_2H_5CF_3SO_3$ to either **1a** or **1b** in THF generates dark red solutions of {**6a**}{OTf} and {**6b**}{OTf}, both of which can be isolated in > 90% yield. Their *S* = 1 spin states (μ_{eff} = 2.79 μ_B for **6a** and 3.0 μ_B for **6b**) are consistent with TBP structures, as confirmed by XRD analysis (τ = ~0.9 for **6a**, 0.96 for **6b**, Figure 4). Their solid-state structures reveal in each case a hydrazine ligand η^1 coordinated to a 5-coordinate iron center in an axial site opposite the silyl anchor. For comparison, diamagnetic and 6-coordinate η^2-hydrazine iron(II) complexes have been reported utilizing bidentate phosphine ligands.ii,xvii,xviii As indicated by Figure 4, the hydrazine moieties in {**6a**}{OTf} and {**6b**}{OTf} are hydrogen-bonded to the triflate anions in the solid-state, with average N-O distances of ~ 3 Å. In **6b**, the hydrogen atoms could be located in the difference map at an average distance of ~ 2 Å for N-H···O. The N-H vibrations for these complexes show the presence of hydrogen bonds in the IR. These vibrations are broadened and shifted in solid-state spectra from that of their non-hydrogen bonded hydrazine derivatives {**6a**}{$B(ArF)_4$} and {**6b**}{$B(ArF)_4$}. Hydrazine adducts with an η^1-binding mode to 5-coordinate metal complexes are uncommon.iv,xix,xx,xxi,xxii,xxiii,xxiv To our knowledge, the only other example of such a species showing approximate three-fold symmetry akin to **6a** and **6b** is a vanadium hydrazine complex supported by a tris(thiolate)amine ligand.xxv

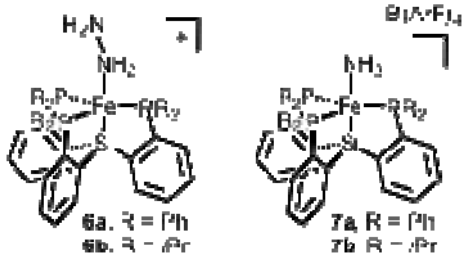

The hydrazine ligand is quite labile for both **6a** and **6b**, and binding of the triflate anion with concomitant release of N_2H_4 can be observed by NMR spectroscopy in C_6D_6. Lability at the apical site, while potentially useful for a catalytic system, is problematic with regard to

attempts to generate an Fe(HN=NH) complex via oxidation of **6a** and **6b**. For instance, our attempts to oxidize these hydrazine complexes with $Pb(OAc)_4$ instead afforded mixtures of the neutral {(SiP^R_3)Fe(OTf)}xvi and {(SiP^R_3)Fe(OAc)} complexes (see SI). Perhaps more interesting is that **6b** can be fully oxidized to $\{(SiP^{iPr}_3)Fe^{II}(N_2)\}^+$ by 3,5-di-*tert*-butyl-*o*-benzoquinone.xxvi

By analogy to the conversion of **6a** and **6b**, a THF solution of ammonia reacts with either **2a** or **3** to afford the corresponding cationic ammonia adducts $\{(SiP^{Ph}_3)Fe^{II}(NH_3)\}\{B(ArF)_4\}$, (**7a**), and $\{(SiP^{iPr}_3)Fe^{II}(NH_3)\}\{B(ArF)_4\}$, (**7b**), Figure 4. The NH_3 ligand is substitutionally labile and hence obtaining rigorously pure samples by thorough drying is challenging: solvents in which the compounds dissolve (e.g., THF) partially substitute the NH_3 ligand. Triplet **7b** (μ_{eff} = 3.27 μ_B) has been structurally characterized and as for the hydrazine derivatives features an NH_3 ligand in the apical site opposite the silyl donor. While its structure (Figure 4) is unremarkable, it serves to underscore that the apical site of the {(SiP^{iPr}_3)Fe} system can accommodate N_2 in the 0, +1, and +2 oxidation states, whereas NH_3 ligation appears accessible only in the +2 oxidation state. Indeed, if one tries to reduce either **7a** or **7b**, NH_3 is quantitatively released and the Fe(I)-N_2 adducts **4a** and **4b** are generated, respectively. The significance of this transformation lies in the ability to recycle Fe(I)-N_2 with release of NH_3, key to the ultimate viability of a hypothetical Fe(I)-N_2 catalyst system for generating ammonia. Also of note is that the reduction of the hydrazine adducts **6a** and **6b** leads to facile generation of **4a** and **4b**, respectively. In these cases, both N_2H_4 and NH_3 are generated as determined by vacuum transfer of the volatiles.

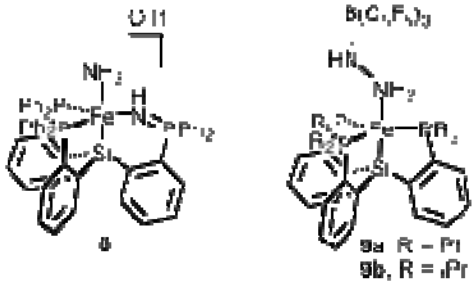

A rare N_XH_y ligand for iron that we sought within this system is the hydrazido ($N_2H_3^-$) ligand.iii We reasoned that the hydrazine adducts **6a** and **6b** might afford access to such complexes via deprotonation. While this did not turn out to be the case, the reaction that results is interesting. When a THF solution of **6a**{OTf} is exposed to a stoichiometric equiv of N^1,N^1,N^8,N^8-tetramethylnaphthalene-1,8-diamine (proton sponge) a reaction ensues affording the paramagnetic ammonia adduct complex {[(Si(*o*-$C_6H_4PPh_2)_2$(*o*-$C_6H_4P(=NH)Ph_2$)]Fe(NH_3)}{OTf}, (**8**), which has been identified by XRD analysis. Its structure reveals that one arm of the SiP^{Ph}_3 ligand is oxidized to P(V) via formal insertion of NH into the Fe-P bond. The N=P bond distance in **8** of 1.5945(1) Å is very close to other reported N=P double bonds.xxvii,xxviii,xxix,xxx,xxxi,xxxii IR spectroscopy shows N-H vibrations at 3339, 3256 and 3168 cm^{-1}. Complexes **6a** and **8** are hence structural isomers of one another and the role of the base thereby appears to be catalytic. The details of this reaction are, however, unclear and complicated by the presence of unidentified byproducts.

While the terminally bonded $N_2H_3^-$ ligand is elusive for these {(SiP_3)Fe} systems, such a ligand can be generated in the presence of the Lewis Acid acceptor $B(C_6F_5)_3$. Thus, the addition of $(C_6F_5)BNH_2NH_2$ to **1a** or **1b** leads to the formation of the neutral and zwitterionic iron(II) hydrazido-borane complexes (SiP^{Ph}_3)Fe^{II}($N_2H_3B(C_6F_5)_3$) (**9a**) and (SiP^{iPr}_3)Fe^{II}($N_2H_3B(C_6F_5)_3$) (**9b**), Figure 4. The hydrazine-borane adduct $N_2H_4B(C_6F_5)_3$ was synthesized from the 1:1 mixture of hydrazine and tris(pentafluorophenyl)borane in THF. Both **9a** and **9b** give easily resolved ^{19}F NMR signals at −123, −157, −162 ppm despite their triplet ground states (μ_{eff} = 2.90 μ_B and 2.83 μ_B). Solid-state crystal structures reveal η^1-bound hydrazido-borane ligands with the borane terminating the β–NH (see Figure 4). To our knowledge, this ligand type is unique.

The B-N bonds (1.544(5) Å for **9a** and 1.553(3) Å for **9b**) are much shorter than that of the precursor $N_2H_4B(C_6F_5)_3$ (1.6316(19) Å). The N-N bond distances are 1.449(4) and 1.442(10) Å for **9a** and **9b**, respectively, which are slightly shortened from that in free $N_2H_4B(C_6F_5)_3$. Interestingly, hydrogen bonds between the hydrogen atoms of hydrazine (and hydrazido) and ortho-fluorine atoms of $B(C_6F_5)_3$ are exhibited in **9a** and **9b**, and also in the precursor $N_2H_4B(C_6F_5)_3$, Figure 4. These intra-molecular N–H···F-C hydrogen bonds are relatively unusual examples of hydrogen bonding in the literature.xxxiii,xxxiv,xxxv,xxxvi,xxxvii All H-bonded H-atoms can be located from the difference maps of the corresponding X-ray crystallographic data, and display distances in the H…F hydrogen bond range; 2.158 Å ~ 2.356 Å.

Synthesis and characterization of Fe-N_2Ph and Fe-N_2SiMe_3

To attempt the synthesis of a mono-substituted hydrazido derivative the methyl complex **1a** was exposed to phenylhydrazinium triflate, Figure 5. The reaction instead afforded a mixture of species presumed to contain paramagnetic {(SiP^{Ph}_3)Fe(NH_2-NHPh)}{OTf} and (SiP^{Ph}_3)Fe(OTf). To try to isolate a well-defined Fe^{II}(NH-NHPh) species the addition of base was pursued. However, while addition of base appears to remove H^+ it also triggers formal loss of H_2 to afford the phenyldiazenido complex {(SiP^{Ph}_3)Fe($N_2C_6H_5$)}, (**10**). This is true for bases such as proton sponge and also phenylhydrazine, PhNH-NH_2, which is necessarily present in solution. Dark brown crystals of **10** can be isolated from the reaction mixture in good yield (~ 70%, Figure 5), and IR spectroscopy reveals an N-N vibration at 1623 cm^{-1}. The solid-state crystal structure (Figure 5) confirms an η^1-phenyldiazenido ligand in an axial position trans to the silyl donor, with short N-N and Fe-N distances (1.233(7) and 1.690(5) Å) reflecting multiple bond character in each linkage. The N-N-C angle (122.5(5)°) establishes sp^2 hybridization at N_β. Diazenido **10** is structurally distinct by virtue of having a diazenido ligand occupying an axial position of a TBP geometry. For the few 5-coordinate iron diazenido complexes that have been structurally characterized, the diazenido ligand occupies an equatorial site.xxxviii,xxxix,xl,xli

The reaction of {(SiP^{Ph}_3)Fe(THF)}{$B(ArF)_4$} **2a** and phenyl hydrazine gives a red solution of {(SiP^{Ph}_3)Fe(NH_2-NHPh)}$^+$, with hydrazine like ^{1}H-NMR signatures based on comparison with the spectra of **6a** and **6b**. N-H vibrations are observed at 3346, 3271, 3230 cm^{-1}. The red product is unstable and is slowly converted to the ammonia adduct **7a** at RT presumably as a result of disproportionation of the iron-bound phenylhydrazine. The major

organic product is aniline, as identified by ^{1}H-NMR and GC. Use of an excess of phenylhydrazine instead gave rise to the inky black product $[(SiP^{Ph}_3)Fe(N_2C_6H_5)]^+$ (**11**). The same product is also obtained by the addition of $\{Cp_2Fe\}\{B(ArF)_4)\}$ to **10** in C_6D_6 solution. The N-N vibrational frequency of **11** is 1690 cm^{-1}, revealing comparatively less back donation from iron to the N-N π* orbital than for **10**. This is also supported by the solid-state structure of **11**, which shows a shorter N-N bond distance and a longer Fe-N bond distance than for **10** (Figure 5). Harder to explain is the curious lengthening of the Fe-P bond distances upon oxidation of **10** to **11**.

Our isolation of the phenyldiazenido complexes **10** and **11** motivated us to explore whether we might be able to prepare related diazenido complexes by direct functionalization of the iron-bound N_2 ligand in the neutral adduct complexes **4a, 4b** or the anion **5**. Whereas we have previously shown that the N_2 ligand in **4a** can be protonated in modest yield to release hydrazine (46% in the presence of $CrCl_2$), trapping a derivatized N_2 ligand still bound to the iron center has proven elusive for the phenyl decorated $(SiP^{Ph}_3)Fe$ system. When $H(OEt_2)_2(B(ArF)_4)$ or CH_3OTf are added to **5** in THF at low temperature, thermally unstable and as yet uncharacterized species appear that eventually decay to the iron(I) N_2 adduct **4b**. At this stage we can only speculate as to the presence of Fe-N_2H and Fe-N_2Me intermediates. The use of silyl electrophiles has proven more fruitful with regard to isolation of products. Thus, treatment of **5** with TMSCl or TMSOTf in frozen THF followed by gradual warming of the solution affords the desired dark red diazenido complex $(SiP^{iPr}_3)Fe(N_2SiMe_3)$ (**12**) with concomitant salt elimination, Figure 6. Complex **12** can also be generated directly from **4b** if Na/Hg amalgam is used as a reductant in the presence of TMSCl. The analogous complexes $(SiP^{iPr}_3)Fe(N_2Si^iPr_3)$ and $(SiP^{iPr}_3)Fe(N_2SiPh_3)$ are obtained using triisopropylsilyl trifluoromethanesulfonate (TIPS-OTf) and triphenylsilyl chloride, respectively. In contrast to its S = 1 relative **10**, diazenido **12** is diamagnetic. Two ^{29}Si-NMR resonances are present in the ^{29}Si-NMR spectrum at 84.3 ppm (q, $^{2}J_{SiP}$ = 38 Hz) and −15.6 ppm (s). A ^{15}N-NMR spectrum of the labeled complex **12-^{15}N** shows two resonances at 418.5 and 270.9 ppmxlii shifted from corresponding peaks for the ^{15}N-enriched precursor **5-^{15}N** (340.3 and 309.7 ppm). Large separation between these two ^{15}N signals is fully consistent with functionalization at the dinitrogen ligand by the TMS group, as for the related molybdenum complex $[HIPTN_3N]$Mo-NNH species.xliii The N-N vibrational frequency of **12** is 1748 cm^{-1} (1694 cm^{-1} for **12**-^{15}N).

Dark red crystals of **12** were obtained and an XRD analysis reveals a TMS group bound to N_β of the TBP iron scaffold (τ = 0.93; Figure 6). The relatively short Fe-N1 distance (1.695(2) Å) implies multiple bond character between the iron center and N_α. The N-N bond distance of 1.195(3) Å establishes further reduction of the N_2 unit relative to its precursor **5** (1.147(4) Å), where a Na^+ cation interacts with N_β. A single point DFT calculation (see SI for details) of **12** illuminates the multiple bond character between iron and N_α nicely, revealing that both HOMO and HOMO-1 possess significant π bonding character between the Fe and N atoms (Figure 6). The difference in magnetic behavior between diazenidos **10** and **12** is curious and is the subject of ongoing studies in our lab. We tentatively suggest that complex **12** is best formulated as a d^8 iron anion, akin to **5** and **5'**, that strongly backbonds into the $N_2SiMe_3^+$ π* orbitals. Such a configuration for a TBP structure is expected to

produce a diamagnet. By contrast, perhaps **10** is better formulated as a d^6 iron center, which for a TBP structure provides a spin triplet in accord with the numerous other $S = 1$ TBP iron(II) complexes described herein. The angle $\angle N_\alpha$-N_β-Si (165.6(3)°) for **12** is far less bent than the $\angle N_\alpha$-N_β-C in complex **10** (122.5(5)°), which is consistent with this comparative description.

To better evaluate the relative state of oxidation of the diamagnetic diazenido species **12** by comparison to the other $(SiP^{iPr}_3)Fe$ species described herein we collected Mössbauer spectra for solid samples of $(SiP^{iPr}_3)Fe(Cl)$, $(SiP^{iPr}_3)Fe(N_2)^+$ (**3**), $(SiP^{iPr}_3)Fe(N_2)$ (**4b**), $\{(SiP^{iPr}_3)Fe(N_2)\}\{Na(THF)_3\}$ (**5**), $\{(SiP^{iPr}_3)Fe(N_2)\}\{Na(12\text{-}C\text{-}4)_2\}$ (**5'**), and $(SiP^{iPr}_3)Fe(N_2SiMe_3)$ (**12**) in zero external magnetic field at 77 K. Each of the spectra shows single quadrupole doublets as shown in Figure 7. Their isomer shifts and quadrupole splittings are listed in Figure 7. The isomer shift of cationic **3** is very close to that of $(SiP^{iPr}_3)Fe(Cl)$ ($S = 1$) and consistent with other ferrous complexes.ix The isomer shift decreases by ca. 0.1 to 0.15 mm/s per formal state of oxidation from **3** to **4b**, and from **4b** to **5** and **5'**. The isomer shift of the silyldiazenido species **12** is closer to that of **5** than **5'** in accord with our supposition that the TMS group capping the N_2 ligand is electronically comparable to the $Na(THF)_3^+$ cation. Therefore, an Fe(0) d^8 assignment is best accorded to complex **12**, at least to the extent that such an assignment is appropriate for diamagnetic **5** and **5'**. Because these complexes are highly covalent our primary intent here is to compare their relative states of oxidation with respect to one another.

In summary, the $\{(SiP^R_3)Fe\}$ scaffold continues to show its effectiveness in stabilizing nitrogenous donor ligands in the apical site of a trigonal bipyramid, trans to the silyl anchor of the ligand auxiliary. In particular, terminal N_2 binding is structurally established for the formal oxidation states Fe(0), Fe(I), and Fe(II). In addition, all of the 5-coordinate iron(II) structures described herein are open shell triplets. The synthesis of open-shell Fe-N_xH_y systems is of timely interest for comparison of their spectroscopic parameters with related data being obtained for the cofactor of nitrogenase under catalytic turnover conditions. The demonstration that the $\{(SiP^R_3)Fe\}$ scaffold can accommodate N_2, NH_3, and N_2H_4 in the apical site, and that $(SiP^R_3)Fe^{II}$-NH_3^+ and $(SiP^R_3)Fe^{II}$-$N_2H_4^+$ species can be recycled to $(SiP^R_3)Fe^I$-N_2 via chemical reduction with concomitant liberation of NH_3, suggests to us that an iron-mediated nitrogen fixation catalyst system based upon three-fold symmetry may yet be accessible. A promising lead is that the iron-bound N_2 ligand reacts with electrophiles at the Fe(0) state, which for the silyl derivatives afford stable Fe-N_2SiR_3 diazenido products.

Supplementary Material

Refer to Web version on PubMed Central for supplementary material.

Acknowledgments

We acknowledge the NIH (GM-070757). Funding for the MIT Department of Chemistry Instrumentation Facility has been provided in part by the NSF (CHE-0234877). Dr. Peter Mueller provided assistance with XRD analyses. NPM is grateful for an NSF graduate fellowship. We thank Professors R. H. Holm and T. A. Betley at Harvard University for providing us with generous access to a Mössbauer spectrometer.

References

i. Saouma CT, Müller P, Peters JC. Characterization of structurally unusual diiron N_xH_y complexes. J Am Chem Soc. 2009; 131:10358–10359. [PubMed: 19722612]

ii. Field LD, Li HL, Magill AM. Base-Mediated Conversion of Hydrazine to Diazene and Dinitrogen at an Iron Center. Inorg Chem. 2009; 48:5–7. [PubMed: 19046077]

iii. Crossland JL, Balesdent CG, Tyler DR. Intermediates in the reduction of N_2 to NH_3: synthesis of iron η^2 hydrazido(1-) and diazene complexes. Dalton Trans. 2009:4420–4422. [PubMed: 19488434]

iv. Sellmann D, Shaban SY, Heinemann FW. Syntheses, Structures and Reactivity of Electron-Rich Fe and Ru Complexes with the New Pentadentate Ligand Et_2NpyS_4-H_2 {4-(Diethylamino)-2,6-bis[(2-mercaptophenyl)thiomethyl]pyridine}. Eur J Inorg Chem. 2004:4591–4601.

v. Peters, JC.; Mehn, MP. Activation of Small Molecules Ch 3. Wiley-VCH; Weinheim: 2006.

vi. Barney BM, et al. Diazene (HN=NH) Is a Substrate for Nitrogenase: Insights into the Pathway of N_2 Reduction. Biochemistry. 2007; 46:6784–6794. [PubMed: 17508723]

vii. Barney BM, et al. A methyldiazene (HN=N-CH_3)-derived species bound to the nitrogenase active-site FeMo cofactor: Implications for mechanism. Proc Natl Acad Sci USA. 2006; 103:17113–17118. [PubMed: 17088552]

viii. Barney BM, et al. Intermediates Trapped during Nitrogenase Reduction of N≡N, CH_3–N=NH, and H_2N–NH_2. J Am Chem Soc. 2005; 127:14960–14961. [PubMed: 16248599]

ix. Hendrich MP, Gunderson W, Behan RK, Green MT, Mehn MP, Betley TA, Lu CC, Peters JC. On the feasibility of N_2 fixation via a single site Fe^{I}/Fe^{IV} cycle - Spectroscopic studies of $Fe^{I}(N_2)Fe^{I}$, Fe^{IV}≡N, and related species. Proc Natl Acad Sci U S A. 2006; 103:17107–17112. [PubMed: 17090681]

x. MacBeth CE, Harkins SB, Peters JC. Synthesis and Characterization of Cationic Iron Complexes Supported by the Neutral Ligands $NP^{i\text{-}Pr}_3$, $NArP^{i\text{-}Pr}_3$, and$NS^{t\text{-}Bu}_3$. Can J Chem. 2005; 83:332–340.

xi. Hinnemann B, NØrskov JK. Modeling a Central Ligand in the Nitrogenase FeMo Cofactor. J Am Chem Soc. 2003; 125:1466–1467. [PubMed: 12568592]

xii. Mankad NP, Whited MT, Peters JC. Terminal Fe^{I}-N_2 and Fe^{II}…H-C Interactions Supported by Tris(phosphino)silyl Ligands. Angew Chem Int Ed. 2007; 46:5768–5771.

xiii. Betley TA, Peters JC. Dinitrogen Chemistry from Trigonally Coordinated Iron and Cobalt Platforms. J Am Chem Soc. 2003; 125:10782–10783. [PubMed: 12952446]

xiv. Addison AW, Rao TN, Reedijk J, van Rijn J, Verschoor GC. Synthesis, Structure and Spectroscopic Properties of Copper(II) Compounds Containing Nitrogen-Sulfur Donor Ligands; the Crystal and Molecular Structure of Aqua[1,7-bis(*N*-methylbenzimidazol-2′- yl)-2,6-dithiaheptane]copper(II) Perchlorate. J Chem Soc Dalton Trans. 1984:1349–1356.

xv. Yandulov DV, Schrock RR. Studies Relevant to Catalytic Reduction of Dinitrogen to Ammonia by Molybdenum Triamidoamine Complexes. Inorg Chem. 2005; 44:1103–1117. [PubMed: 15859292]

xvi. Whited MT, Mankad NP, Lee Y, Oblad PF, Peters JC. Dinitrogen Complexes Supported by Tris(phosphino)silyl Ligands. Inorg Chem. 2009; 48:2507–2517. [PubMed: 19209938]

xvii. Field LD, Li HL, Dalgarno SJ, Turner P. The first side-on bound metal complex of diazene, HN=NH. Chem Comm. 2008:1680–1682. [PubMed: 18368163]

xviii. Crossland JL, Zakharov LN, Tyler DR. Synthesis and Characterization of an Iron(II) η^2-Hydrazine Complex. Inorg Chem. 2007; 46:10476–10478. [PubMed: 17983220]

xix. Yu Y, Brennessel WW, Holland PL. Borane B–C Bond Cleavage by a Low-Coordinate Iron Hydride Complex and N–N Bond Cleavage by the Hydridoborate Product. Organometallics. 2007; 26:3217–3226. [PubMed: 18725998]

xx. Shakir M, Parveen S, Begum N, Azim Y. Interaction of manganese(II), iron(II), cobalt(II), nickel(II), copper(II) and zinc(II) with acetylhydrazine, formed *in situ*; first crystal structure of tris(acetylhydrazine) nickel(II) perchlorate. Transition Metal Chem. 2004; 29:916–920.

xxi. Albertin G, Antoniutti S, Bordignon E, Chimisso F. Preparation of bis(hydrazine) complexes of iron(II). Inorg Chem Commu. 2001; 4:402–404.

xxii. Sellmann D, Soglowek W, Knoch F, Ritter G, Dengler J. Transition-Metal Complexes with Sulfur Ligands. 88. Dependence of Spin State, Structure, and Reactivity of [Fe^{II}(L)(‘N_HS_4’)] Complexes on the Coligand L (L = CO, N_2H_2, N_2H_4, NH_3, Pyridine, $NHCH_3NH_2$, CH_3OH, THF, $P(OCH_3)_3$, $P(OPh)_3$): Model Complexes for Iron Nitrogenases (‘N_HS_4’$^{2-}$ = Dianion of 2,2‘-Bis[(2- mercaptophenyl)thio]diethylamine). Inorg Chem. 1992; 31:3711–3717.

xxiii. Casey MT, Guinan P, Canavan A, McCann M, Cardin C, Kelly NB. Reaction of 1,1′-diacetylferrocene with hydrazine hydrate: Synthesis and X-ray crystal structures of bis(hydrazine)bis(hydrazinecarboxylato-N′,O)iron(II), [$Fe(N_2H_4)_2(O_2CNHNH_2)_2$], and the cyclic biferrocene diazine, [---N(Me)$CC_5H_4FeC_5H_4$C(Me)N---]$_2$. Polyhedron. 1991; 10:483–489.

xxiv. Goedken VL, Peng S-M, Molin-Norris J, Park Y-A. Carbon monoxide complexes of iron(II): synthesis and structural studies of five- and six-coordinate complexes of the macrocyclic ligand, $C_{22}H_{22}N_4^{2-}$. J Am Chem Soc. 1976; 98:8391–8400. [PubMed: 993530]

xxv. Davies SC, et al. Vanadium Complexes of the $N(CH_2CH_2S)_3^{3-}$ and $O(CH_2CH_2S)_2^{2-}$ Ligands with Coligands Relevant to Nitrogen Fixation Processes. Inorg Chem. 2000; 39:3485–3498. [PubMed: 11196806]

xxvi. It is likely that the N_2 in the product derives from both the original N_2H_4 in the precursor and atmospheric N_2 due to rapid ligand exchange.

xxvii. Alhomaidan O, Hollink E, Stephan DW. Main Group Heterocycles from Lithiated Phosphinimines. Organometallics. 2007; 26:3041–3048.

xxviii. Aguilar D, Contel M, Navarro R, Urriolabeitia EP. Organogold(III) Iminophosphorane Complexes as Efficient Catalysts in the Addition of 2-Methylfuran and Electron-Rich Arenes to Methyl Vinyl Ketone. Organometallics. 2007; 26:4604–4611.

xxix. Bielsa R, Larrea A, Navarro R, Soler T, Urriolabeitia EP. Synthesis, Structure, Reactivity, and Catalytic Activity of *C,N*- and *C,N,N*-Orthopalladated Iminophosphoranes. Eur J Inorg Chem. 2005:1724–1736.

xxx. Chan KTK, et al. Anionic Phosphinimine-Chelate Complexes of Rhodium and Iridium: Steric and Electronic Influences on Oxidative Addition of CH_2Cl_2. Organometallics. 2004; 23:381–390.

xxxi. Spencer LP, et al. Pyridine– and Imidazole–Phosphinimine Bidentate Ligand Complexes: Considerations for Ethylene Oligomerization Catalysts. Organometallics. 2003; 22:3841–3854.

xxxii. LePichon L, Stephan DW, Gao Z, Wang Q. Iron Phosphinimide and Phosphinimine Complexes: Catalyst Precursors for Ethylene Polymerization. Organometallics. 2002; 21:1362–1366.

xxxiii. Mountford AJ, et al. Intra- and Intermolecular N–H···F–C Hydrogen-Bonding Interactions in Amine Adducts of Tris(pentafluorophenyl)borane and –alane. Inorg Chem. 2005; 44:5921–5933. [PubMed: 16060648]

xxxiv. Hyla-Kryspin I, Haufe G, Grimme S. Weak Hydrogen Bridges: A Systematic Theoretical Study on the Nature and Strength of C-H···F-C Interactions. Chem Eur J. 2004; 10:3411. [PubMed: 15252787]

xxxv. Brammer L, Bruton EA, Sherwood P. Understanding the Behavior of Halogens as Hydrogen Bond Acceptors. Cryst Crowth Des. 2001; 1:277.

xxxvi. Takemura H, et al. The C-F···Cation Interaction: An Ammonium Complex of a Hexafluoro Macrocyclic Cage Compound. Chem Eur J. 2000; 6:2334. [PubMed: 10939735]

xxxvii. Howard JAK, Hoy VJ, O’Hagan D, Smith GT. How good is fluorine as a hydrogen bond acceptor? Tetrahedron. 1996; 52:12613.

xxxviii. Davies SC, Hughes DL, Richards RL, Sanders JR. Molybdenum and tungsten complexes of the $N(CH_2CH2S)_3^{3-}$ (NS_3) ligand with oxide, sulfide, diazenide, hydrazide and nitrosyl co-ligands. J Chem Soc Dalton Trans. 2000:719–725.

xxxix. Albertin G, et al. Reactivity of Hydrides $FeH_2(CO)_2P_2$ (P = Phosphites) with Aryldiazonium Cations: Preparation, Characterization, Xray Crystal Structure, and Electrochemical Studies of Mono- and Binuclear Aryldiazenido Complexes. Inorg Chem. 1998; 37:5602–5610. [PubMed: 11670708]

xl. Albertin G, Antoniutti S, Pelizzi G, Vitali F, Bordignon E. Bis(aryldiazene) derivatives of iron(II): preparation, characterization, and properties of the first complexes containing two diazene ligands bonded to the same central metal. The x-ray crystal structures of hexacoordinate [FeH(4-$CH_3C_6H_4NNH)[P(OEt)_3]_4]^+$, and pentacoordinate $[Fe(4\text{-}CH_3C_6H_4N_2)[P(OEt)_3]_4]^+$ cations. J Am Chem Soc. 1986; 108:6627–6634.

xli. Haymore BL, Ibers JA. Aryldiazo complexes. Structure of an iron-aryldiazo complex, dicarbonyl bis(triphenylphosphine) benzenediazonium iron(1+) tetrafluoroborate (1-). Inorg Chem. 1975; 14:1369–1376.

xlii. By ^{29}Si-NMR measurements, ^{15}N-^{29}Si coupling was detected at −15.9 ppm (dd, $^{1,2}J_{SiN}$ = 10, 2.2 Hz).However, no coupling was detected in the ^{31}P-NMR spectrum of the ^{15}N-enriched sample, even at −90 °C

xliii. Yandulov DV, Schrock RR. Reduction of Dinitrogen to Ammonia at a Well-Protected Reaction Site in a Molybdenum Triamidoamine Complex. J Am Chem Soc. 2002; 124:6252–6253. [PubMed: 12033849]

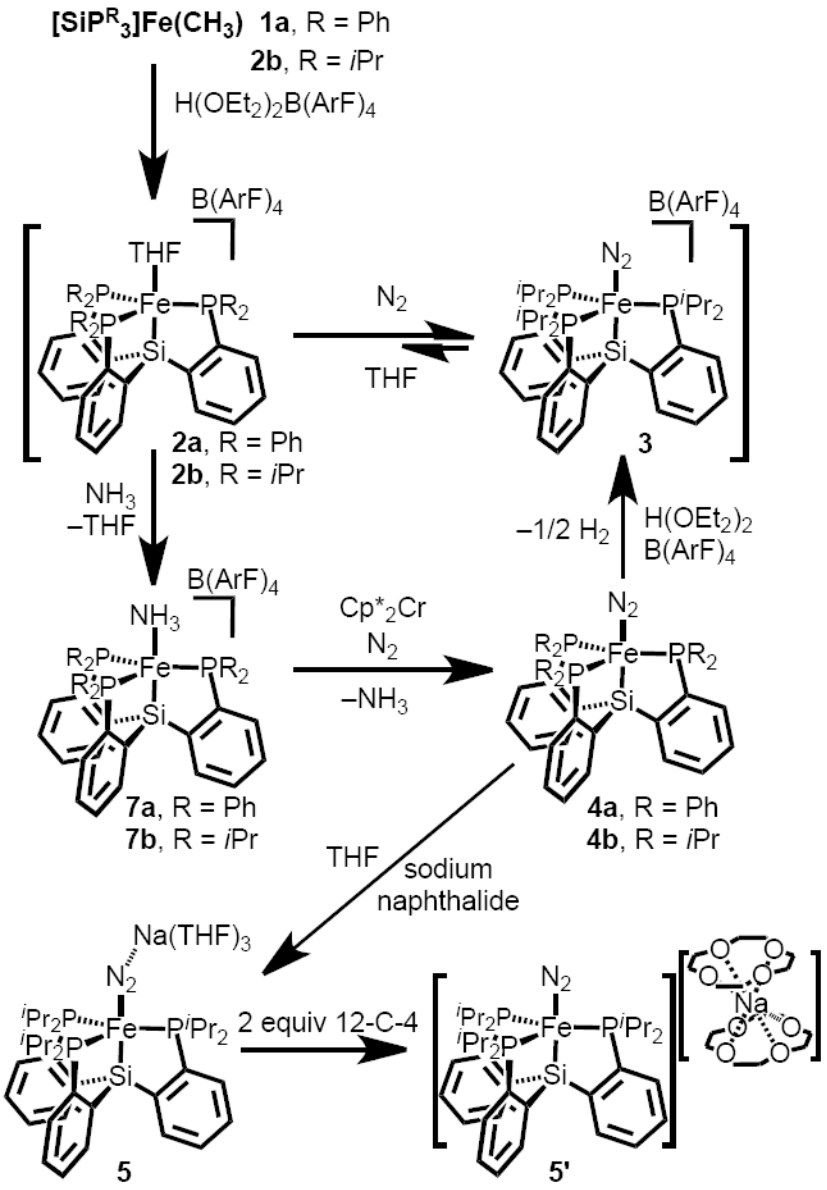

Figure 1. Synthetic scheme for the generation of Fe-N_2^+, Fe-N_2, and Fe-N_2^- (3, 4b, 5 and 5')

Exposure of ammonia to cationic Fe-THF$^+$ (**2a**, R = Ph or **3**, R = *i*Pr) affords the ammonia complexes **7a** and **7b**. Upon addition of Cp*$_2$Cr nitrogen uptake generates Fe-N_2 (**4a** or **4b**) with quantitative release of NH_3. Sodium naphthalide reduction of **4b** generates Fe-N_2^- (**5** and **5'**).

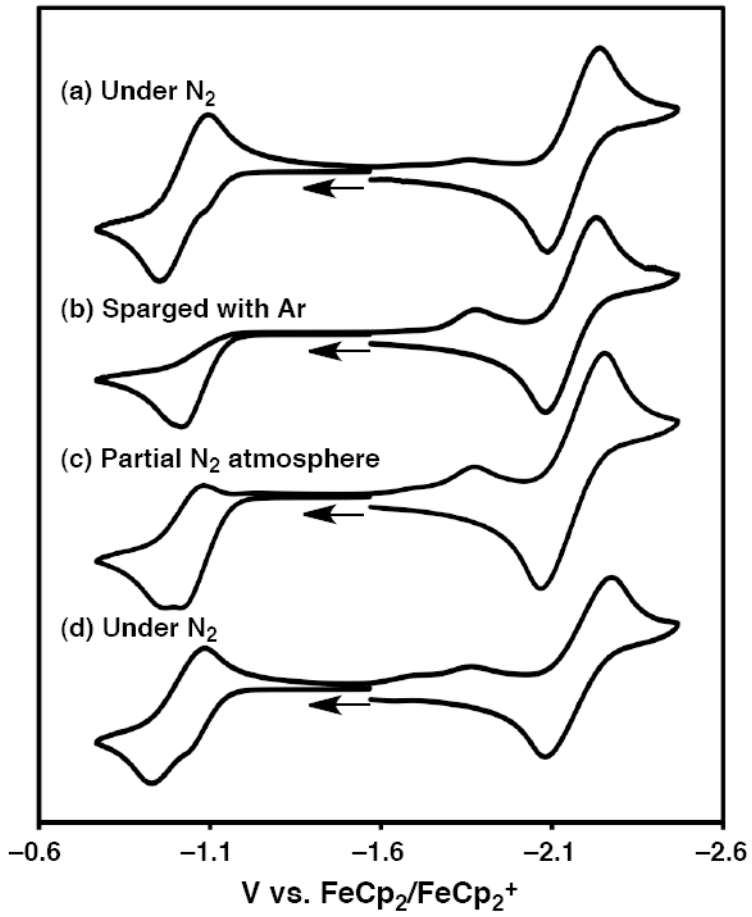

Figure 2. Cyclic voltammetry behavior of (SiP^{iPr}_3)Fe(N_2) (4b)

(**a**) CV under an N_2 atmosphere; (**b**) after sparging sample with argon for 30 sec; (**c**) after partial removal of argon under vacuum and re-exposure to an N_2 atmosphere; (**d**) after another vacuum/N_2 exposure cycle. Data collected in tetrahydrofuran at 100 mV/s and 0.3 M $\{^nBu_4\}\{PF_6\}$.

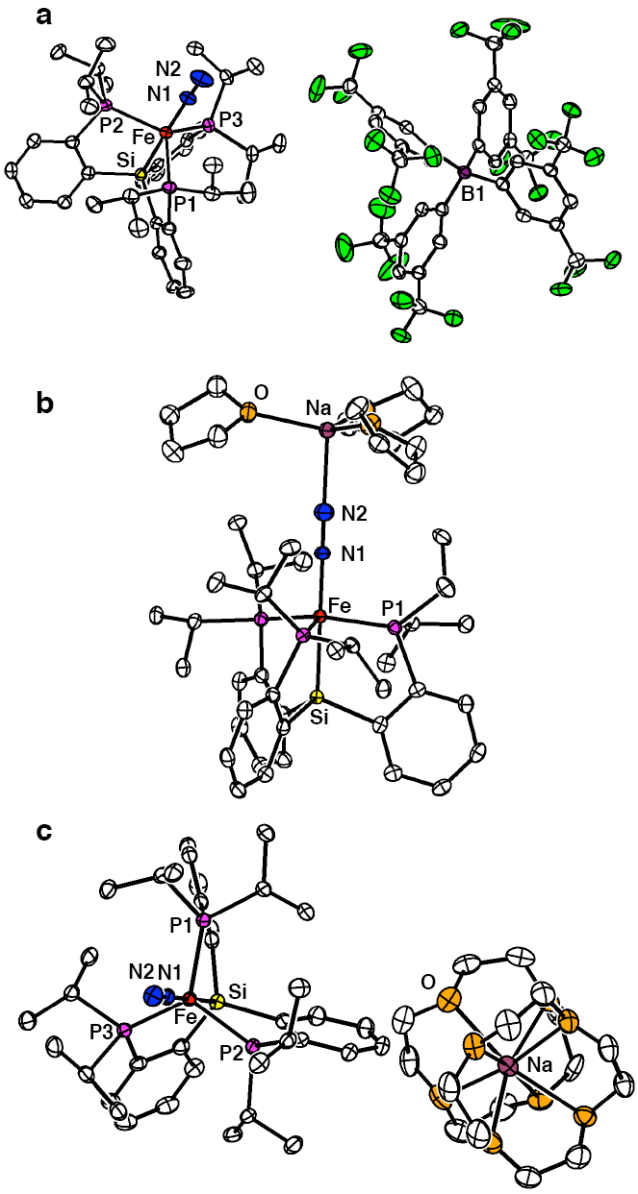

Figure 3. Solid-state structures of 3, 5, and 5'

(**a**) {(SiP$^{i\mathrm{Pr}}_3$)Fe(N_2)}{B(ArF)$_4$} (**3**); (**b**) {(SiP$^{i\mathrm{Pr}}_3$)Fe(N_2)}{Na(THF)$_3$} (**5**); (**c**) {(SiP$^{i\mathrm{Pr}}_3$)Fe(N_2)}{Na(12-C-4)$_2$} (**5'**). All hydrogen atoms and molecules of co-crystallization have been omitted for clarity. See SI for complete details.

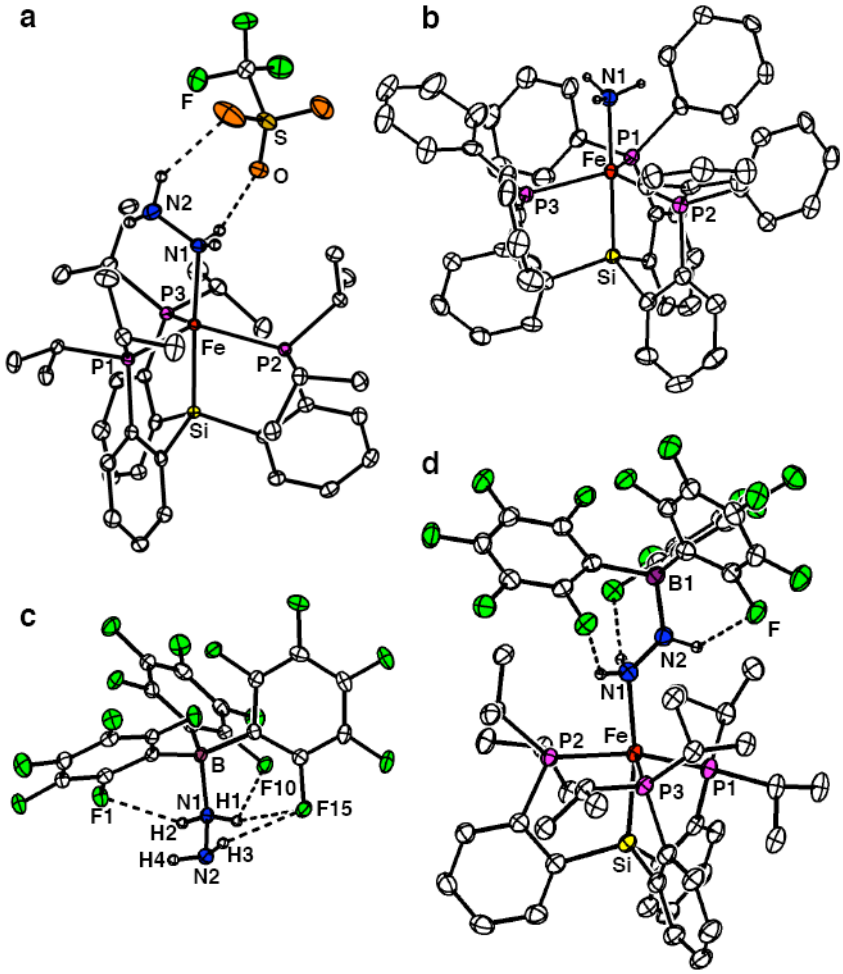

Figure 4. Solid-state structures of {6b}{OTf}, 7a, $N_2H_4B(C_6F_5)_3$, and 9b

(**a**) {(SiP^{iPr}_3)Fe^{II}(N_2H_4)}{OTf} ({**6b**}{OTf}); (**b**) {(SiP^{Ph}_3)Fe^{II}(NH_3)}{$B(ArF)_4$} (**7a**); (**c**) $N_2H_4B(C_6F_5)_3$; (**d**) (SiP^{iPr}_3)Fe^{II}($N_2H_3B(C_6F_5)_3$) (**9b**). Selected hydrogen atoms and the {$B(ArF)_4$} anion of **7a** have been omitted for clarity. See SI for details.

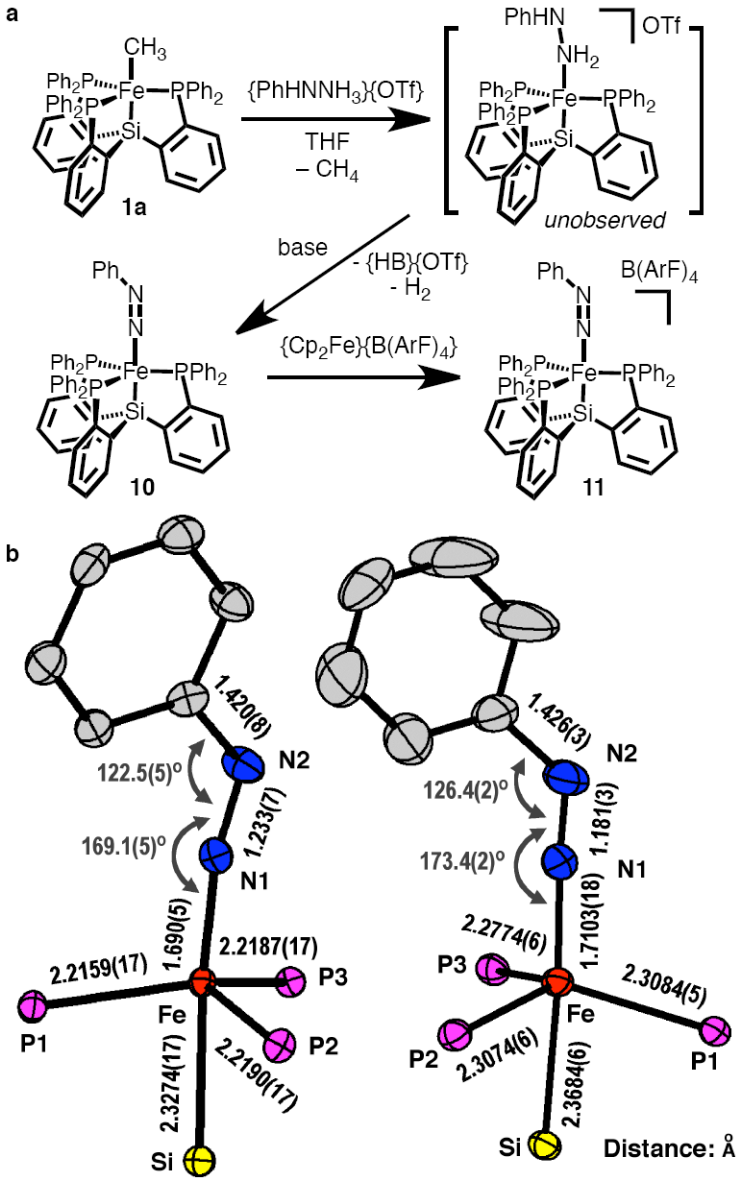

Figure 5. Synthesis and characterization of $(SiP^{Ph}_3)Fe^{II}(N_2C_6H_5)$ (10) and $\{(SiP^{Ph}_3)Fe^{II}(N_2C_6H_5)\}\{B(C_6H_3(CF_3)_2)_4\}$ (11)

(**a**) Synthetic scheme for the generation of **10** and 11; (**b**) Core atom 50% probability ellipsoid representations of the solid-state structures of **10** and **11**.

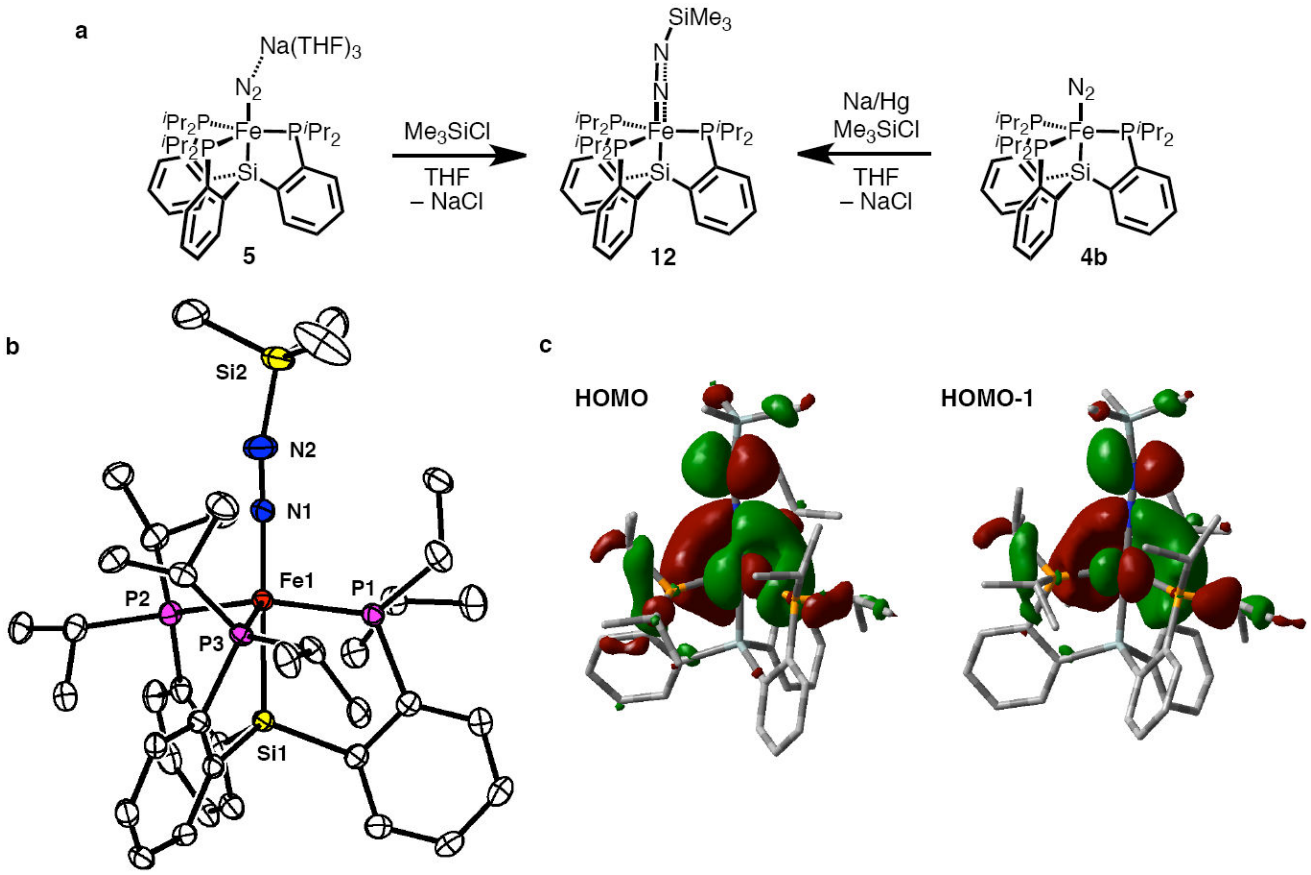

Figure 6. Synthesis and characterization of (SiP^{iPr}_3)Fe^{II}(N_2SiMe_3) (12)

(a) Synthesis of **12** via silylation of **5** or via reductive silylation of **4b**; (**b**) Solid-state structure of **12**. Hydrogen atoms have been removed for clarity. Selected bond distances (Å) and angles (°) for **12**: Fe1-N1 1.695(2), N1-N2 1.195(3), Si2-N2 1.720(3), Fe1-Si1 2.3104(9), Fe1-P1 2.2508(8), Fe1-P2 2.2577(8), Fe1-P3 2.2500(8); P1-Fe1-P2 119.80(3), P2-Fe1-P3 114.28(3), P3-Fe1-P1 116.94(3), N1-Fe1-Si1 175.78(9), N2-N1-Fe1 175.7(3), N1-N2-Si2 165.6(3); (**c**) DFT calculated HOMO and HOMO-1 of **12** (see SI for details).

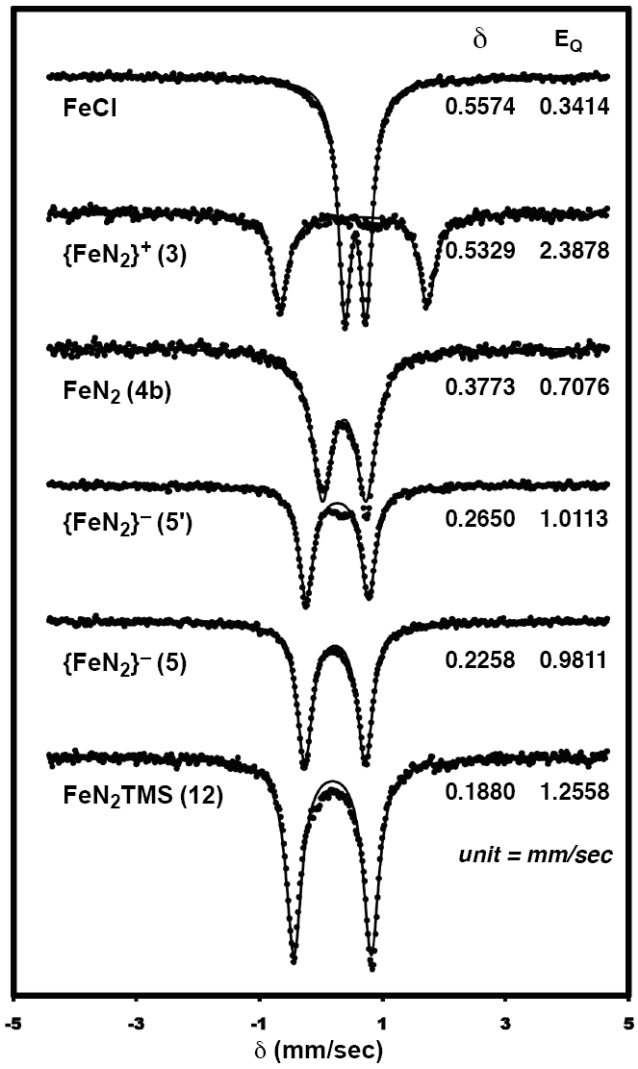

Figure 7. Zero field Mössbauer spectra

Spectra are recorded at 77 K and offset from top to bottom in the following order: $(SiP^{iPr}_3)Fe(Cl)$,[a] $\{(SiP^{iPr}_3)Fe(N_2)\}\{B(ArF)_4\}$ (**3**), $(SiP^{iPr}_3)Fe(N_2)$ (**4b**), $\{(SiP^{iPr}_3)Fe(N_2)\}\{Na(12\text{-}C\text{-}4)_2\}$ (**5'**), $\{(SiP^{iPr}_3)Fe(N_2)\}\{Na(THF)_3\}$ (**5**), and $(SiP^{iPr}_3)Fe(N_2SiMe_3)$ (**12**). The dotted lines are the raw data and the solid lines are fits using the parameters listed. [a]No effect with an applied external magnetic field of 45 mT was observed.

Table 1

Physical parameters for the N_2 adduct species **3, 4b, 5** and **5'**

	{FeN$_2$}{B(ArF)$_4$} 3	**Fe-N$_2$ [d],xvi 4b**	**{FeN$_2$}{Na(THF)$_3$} 5**	**{FeN$_2$}{Na(12-C-4)$_2$} 5'**
ν(NN)[a]	2143	2003	1891	1920
N-N (Å)	1.091(3)	1.1245(2)	1.147(4)	1.132(4)
Fe-N (Å)	1.914(2)	1.8191(1)	1.763(3)	1.795(3)
Fe-Si (Å)	2.298(7)	2.2713(6)	2.2526(9)	2.236(1)
Si-Fe-N (°)	178.63(8)	178.73(5)	180.00(0)	179.8(1)
color[b] nm (M^{-1} cm^{-1})	blue 500 (270) 610 (145)	Red 380 (3500)	Purple 510 (3600)	Purple 520 (3800)
spin- state[c]	3.3 BM S = 1	2.2 BM S = ½	diamagnetic	diamagnetic

[a] KBr pellet;

[b] THF solution;

[c] Evans' Method in THF-d_8 (**3**);

[d] Updated X-ray data. Structure originally reported in ref xvi contains ~ 4% (SiP^{i}Pr$_3$)FeCl.